Frustrated competitive forces in the Et 2 Me 2 Sb[Pd(dmit) 2] 2 molecular conductor

Laurent Guérin, Elzbieta Trzop, Tadahiko Ishikawa, Shinya Koshihara, Takashi Yamamoto, Bertrand Toudic, Reizo Kato

Frustrated competitive forces in the $Et_2Me_2Sb[Pd(dmit)_2]_2$ molecular conductor

Laurent Guérin,[1,2,*] Elzbieta Trzop,[1,2] Tadahiko Ishikawa,[3] Shin-ya Koshihara,[3] Takashi Yamamoto,[4,5,6] Bertrand Toudic,[1,2] and Reizo Kato[6,†]

[1] *Univ. Rennes, CNRS, IPR (Institut de Physique de Rennes) - UMR 6251, F-35000 Rennes, France*
[2] *International Research Laboratory DYNACOM, DYNACOM IRL2015 University of Tokyo - CNRS - Univ. Rennes*
[3] *Department of Chemistry, School of Science, Tokyo Institute of Technology, 2-12-1, Ookayama, Meguro-ku,Tokyo 152-8551, Japan*
[4] *Graduate School of Science and Engineering, Ehime University, 2-5, Bunkyoucho, Matsuyama 790-8577, Japan*
[5] *Geodynamics Research Center, Ehime University, 2-5, Bunkyoucho, Matsuyama 790-8577, Japan*
[6] *Condensed Molecular Materials Laboratory, RIKEN, 2-1 Hirosawa, Wako, Saitama 351-0198, Japan*

(Dated: September 19, 2023)

The $Et_2Me_2Sb[Pd(dmit)_2]_2$ salt is a Mott insulator at room temperature with layers of equivalent dimers $[Pd(dmit)_2]_2$ forming a 2D triangular lattice. Although spin liquid behavior has been reported in other systems with a quasi-triangular lattice, $Et_2Me_2Sb[Pd(dmit)_2]_2$ shows no spin liquid behavior irrespective of the expected high spin frustration due to its almost perfect equilateral triangular structure. Here, we report a high resolution structural analysis that reveals the existence of an intermediate incommensurate phase between the highly frustrated room temperature phase and the charge separated phase characterized by differently charged dimers coupled to different intradimer Pd-Pd distances. The structure of the incommensurate phase exhibits no modulation of the Pd-Pd distance but a large steric effect between the cation and the terminal sulfur atom of the $Pd(dmit)_2$ molecules. In addition to this steric frustration, the interdimer transfer integrals coupled to the arch-distortion in the dimer are also modulated suggesting that the spin state in the incommensurate phase is ascribed to an incommensurate modulation of the transfer integral. We demonstrate that the presence of the incommensurate phase originates from different frustrated competitive forces and discuss its magnetic and optical properties.

I. INTRODUCTION

The charge transfer complexes consisting of a $Pd(dmit)_2$ (dmit = 1,3-dithiole-2-thione-4,5-dithiolate) anion, $Z[Pd(dmit)_2]_2$ (Z = monovalent cation), exhibit diverse phases such as metal, dimer Mott insulator, charge separation (CS), valence bond liquid, and valence bond solid [1–3]. These phases arise from the competition of interactions among charges and spins in a two-dimensional triangular lattice that can lead to frustration [4–9]. Geometrical frustration results in a highly degenerate ground state, where numerous spin arrangements are energetically equivalent. This can give rise to a range of interesting phenomena, including the emergence of exotic phases and excitations, appearance of incommensurate phases, as well as a suppression of long-range orders [10, 11]. The discovery of quantum spin liquids (QSLs) has brought attention to quasi-two-dimensional molecular crystals as they form highly frustrated triangular arrangements of dimers occupied by a single charge with spin 1/2 [6, 12–14].

The compound $Et_2Me_2Sb[Pd(dmit)_2]_2$, shown in Fig. 1(a), belongs to such a strongly correlated two-dimensional system [1, 2, 15]. The crystal structure of $Et_2Me_2Sb[Pd(dmit)_2]_2$ consists of alternately stacked anion layers composed of $Pd(dmit)_2$ and insulating cation layers [Fig. 1(b)]. At room temperature, it crystallizes in the monoclinic C2/c space group (a = 14.62 Å, b = 6.40 Å, c = 37.51 Å, β = 97.72 ° at 250 K). The unit cell contains two conduction layers related to each other by the c-glide symmetry. Each layer lies parallel to the ($\boldsymbol{a}$, $\boldsymbol{b}$) plane and is composed of crystallographic equivalent $Pd(dmit)_2$ molecules stacking along the $\boldsymbol{a}$+$\boldsymbol{b}$ or $\boldsymbol{a}$-$\boldsymbol{b}$ direction. Due to the strong dimerization of the $Pd(dmit)_2$ molecules, the dimer has been considered as an effective unit. At room temperature, $Et_2Me_2Sb[Pd(dmit)_2]_2$ is a dimer Mott insulator, with a uniform charge of -1 (monovalent) on each $[Pd(dmit)_2]_2$ dimers. The formal charge of the $Pd(dmit)_2$ molecule in these salts is -0.5, and the system has a half-filled character owing to the tight dimerization [16, 17], as shown in Fig. 1(c). This ($\boldsymbol{a}$, $\boldsymbol{b}$) anion layer can be described as an equilateral triangular lattice with an anisotropy parameter J_r/J = 1 [15], where J_r and J represent interdimer HOMO-HOMO transfer integrals [Fig. 1(c)]. Around 70 K, $Et_2Me_2Sb[Pd(dmit)_2]_2$ undergoes a phase transition, as indicated by the temperature dependence of the magnetic susceptibility in Fig. 1(d). The space group changes to monoclinic $P2_1/c$ (a' = 14.50 Å, b' = 12.65 Å, c' = 37.18 Å, β' = 98.09 ° at 25 K). The low temperature structure consists of dimers with distinct valence states arranged alternatively along the $\boldsymbol{b}$ direction. This indicates that the phase transition is associated with CS, where loose divalent and tight neutral dimers are ordered [Fig. 1(c)].

The origins of QSL have been a subject of debate and the contradiction that a candidate of QSL does not necessarily have an equilateral triangular lattice has remained unclear. $Et_2Me_2Sb[Pd(dmit)_2]_2$ and

* laurent.guerin@univ-rennes.fr
† reizo@riken.jp

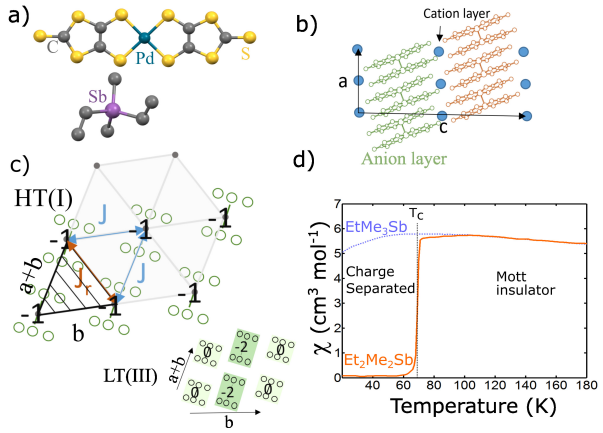

FIG. 1. (a) The complex molecule Pd(dmit)$_2$ and the Et_2Me_2Sb cation. (b) Schematic representation of the ($\boldsymbol{a}$,$\boldsymbol{c}$) plane showing cation layers and anion layers perpendicular to the $\boldsymbol{c}$ axis. (c) Schematic representation of the (a,b) showing the anion layer (in green) in the high temperature (HT) and low temperature (LT) phases. The anion layer in the HT phase forms a triangular lattice of monovalent dimers. The unit cell (hashed area) axis are along $\boldsymbol{a}$+$\boldsymbol{b}$ and $\boldsymbol{b}$ direction. J_r and J are the interdimer transfer integrals. Tight neutral and loose divalent dimers are formed in the LT phase. (d) Temperature dependence of the magnetic susceptibility (red solid line) in $Et_2Me_2Sb[Pd(dmit)_2]_2$ and a candidate of quantum spin liquids $EtMe_3Sb[Pd(dmit)_2]_2$ as a reference compound (blue dotted line).

$EtMe_3Sb[Pd(dmit)_2]_2$ present a very similar structure but behave much differently, with the latter being in a QSL state at low temperature [12]. The quasi-two-dimensional molecular crystal $Et_2Me_2Sb[Pd(dmit)_2]_2$ forms highly frustrated triangular arrangements of dimers, which closely resemble an equilateral triangular lattice. This motivates a detailed analysis in order to understand the different competitive forces associated with the frustration in a triangular lattice. In this paper, we focus on the temperature range between 105 and 65 K where the magnetic susceptibility exhibits an unexplained behavior [Fig. 1(d)]. Furthermore, diffuse satellite reflections were previously reported at 90 K [2] and we demonstrate that they are linked to the emergence of an incommensurate phase. We collected high resolution X-ray diffraction data at various temperatures and we employed the superspace formalism to characterize this phase and solved the structure in the superspace. The structure of the incommensurate phase and its infrared vibrational spectrum can be interpreted in terms of the competition between different steric, electronic and magnetic interactions.

II. EXPERIMENTAL SECTION

Single crystals of $Et_2Me_2Sb[Pd(dmit)_2]_2$ were prepared by the air oxidation method [15]. Their structural analysis was done by X-ray diffraction experiments performed on single crystals. The diffraction experiments were carried out on a Xcalibur3 four-circle diffractometer (Oxford Diffraction) equipped with a 2D sapphire3 CCD detector and Mo-Kα radiation. High resolution diffraction experiments were also performed using monochromated Cu-Kα radiation from a rotating anode source and a high resolution mar345dtb imaging plate (Marresearch GmbH), which was placed as far as 400 mm from the crystal to spatially resolve the Bragg peaks. Crysalis Pro software from Oxford Diffraction [18] was used to reduce the data. The low temperature X-ray diffraction experiments were performed with a constant gas flow helium cryostat. The periodic structures at 250 and 25 K were solved by direct methods using SHELXT [19]. Here data were refined by full-matrix least squares on F2 using SHELXL [19, 20], All non-hydrogen atoms were refined anisotropically and H-atoms were constrained by geometry. CCDC-2269860 and CCDC-2269862 contain the supplementary crystallographic data for 250 and 25 K respectively [21].

III. THE SEQUENCE OF PHASES OF $Et_2Me_2Sb[Pd(dmit)_2]_2$

Figure 2(a) presents, between 110 and 15 K, several Mo-Kα diffraction images along the $\boldsymbol{b}^*$ direction. Three differently assigned Bragg peaks are observed. Above 105 K, only Bragg peaks signing the C2/c space group are observed. Between 70 and 100 K, supplementary satellites Bragg peaks are present at a position $\boldsymbol{q_s} = \beta\ \boldsymbol{b}^*$, with β of the order of 0.45 in b^* units. In the low temperature phase, these satellites Bragg peaks become commensurate and additional superstructure Bragg peaks appears. In agreement with reference [2], the space group of this low temperature phase is $P2_1/c$. Figure 2(b) shows the temperature dependence of the incommensurate diffraction Bragg peaks along the $\boldsymbol{b}^*$ direction as a function of the temperature between 100 and 80 K obtained using high resolution diffraction. A clear temperature dependence of the misfit parameter β is shown in Fig. 2(c). The irrational number of the parameter β together with its continuous change as function of temperature is a characteristic feature of an incommensurate modulated phase. The superspace group is determined by the observation of the conditions for main and satellites reflections. In the present case, the mean structure is monoclinic C2/c and the critical wave vector is $\boldsymbol{q_s} = \beta\ \boldsymbol{b}^*$, so the superspace group is C2/c (0β0). For the satellite reflections, an additional extinction rule for reflections 0k0m with m = 2n+1 is observed suggesting the superspace symmetry element s. The only (3+1)-dimensional superspace group in compliance with this condition is C2/c (0 β 0) s0. The superspace groups of dimension four have been systematically discussed in references [22–25]. According to this work, an alternative setting of superspace group B2/b (0 0 γ) s0 corresponding to 15.1.7.3 space-

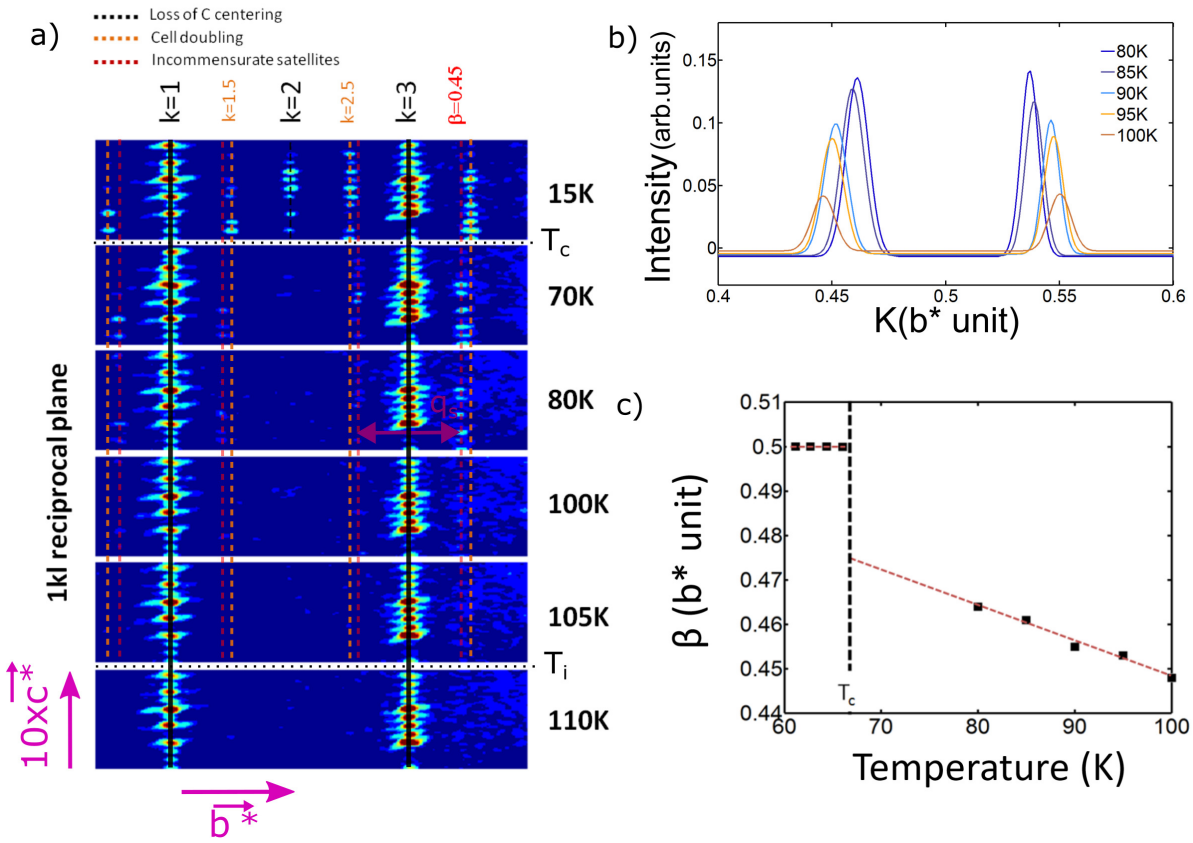

FIG. 2. (a) Diffraction imaging obtained from Xcalibur four-circle diffractometer analysis with Mo-Kα radiation of a single crystal of $Et_2Me_2Sb[Pd(dmit)_2]_2$. The diffraction plane (1, k, l) is shown at several temperatures. The frames at 110 K and 105 K reflects the C2/c symmetry of the high symmetry phase. The images at 100, 80, and 70 K show a supplementary set of satellite Bragg peaks at incommensurate positions $\boldsymbol{q_s} = \beta\ \boldsymbol{b^*}$. The lowest temperature image, at 15 K, shows a cell doubling along b* and the appearance of Bragg peaks signing the loss of the C-centering in agreement with a three-dimensional space group $P2_1/c$. (b) Temperature dependence of incommensurate peaks observed using high resolution diffraction experiments. (c) Temperature evolution of the positions of the satellite Bragg peaks $\boldsymbol{q_s} = \beta\ \boldsymbol{b^*}$.

group can be used. In order to conform to the cell chosen by Nakao et al. [2], the description in C2/c (0 β 0) s0 is used in this article. The actual sequence of three phases of $Et_2Me_2Sb[Pd(dmit)_2]_2$ is shown in Fig. 3. Hereafter, we denote the phase between Ti = 105 K and Tc = 66.5 K as phase II and the previously-reported phases as phases I and III. The phase transition from the monoclinic high symmetry phase I C2/c to the incommensurate one (phase II) is marked by a continuous increase of the intensity of the satellite Bragg peaks. A modulated incommensurate crystal can be seen as a perturbation of a periodic three dimensional lattice by a modulation whose period is in an incommensurate ratio with the periodicity of the mean lattice. The amplitude of the modulation is weak and increases continuously by lowering the temperature leading to a first order lock-in phase transition at Tc = 66.5 K. This lock-in phase, phase III was previously reported as the low symmetry phase $P2_1/c$. The diffraction signature presents two characteristic features. First, a jump from incommensurate satellite vector $\boldsymbol{q_s} = \beta\ \boldsymbol{b^*}$ having an irrational β to commensurate vector $\boldsymbol{q_s} = 1/2\ \boldsymbol{b^*}$. Second, at this temperature, the mean structure lowers the symmetry from C2/c to $P2_1/c$ yielding the appearance of Bragg peaks at h+k odd (Fig. 3). The observed sequence of phases corresponds to the usual sequence of phases in incommensurate modulated crystals with a jump of the incommensurate vector $\boldsymbol{q_s}$ to a commensurate one [26, 27]. In this compound, no study of the incommensurate phase had been done before.

IV. STRUCTURE OF THE INCOMMENSURATE PHASE AS DETERMINED IN A (3+1)-DIMENSIONAL CRYSTALLOGRAPHIC SUPERSPACE

The structure of $Et_2Me_2Sb[Pd(dmit)_2]_2$ within its incommensurate phase (80 K) was solved and refined in a (3+1)-dimensional superspace using SUPERFLIP and JANA Programs [28]. The basic principle of the crystallographic superspace of dimension (3+1) is illustrated in Fig. 4 considering the actual parameters encountered in

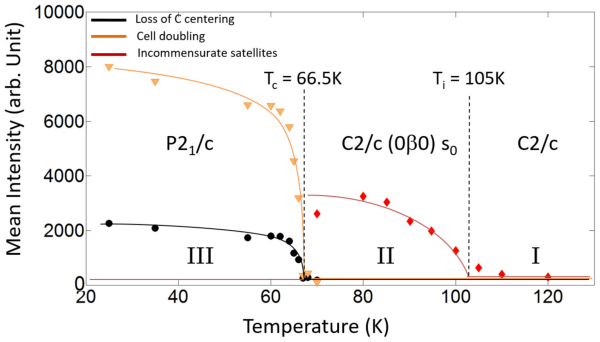

FIG. 3. Phase diagram of $Et_2Me_2Sb[Pd(dmit)_2]_2$ defined by temperature evolution of the intensities of satellite Bragg peaks. Diamonds: intensity of the satellites in the incommensurate phase C2/c $(0\beta0)$s0 defining $Ti = 105$ K. Triangle and circle: Bragg peak intensities signing respectively the cell doubling and the loss of the centering due to the commensurate lock-in phase transition at $Tc = 66.5$ K towards the space group $P2_1/c$.

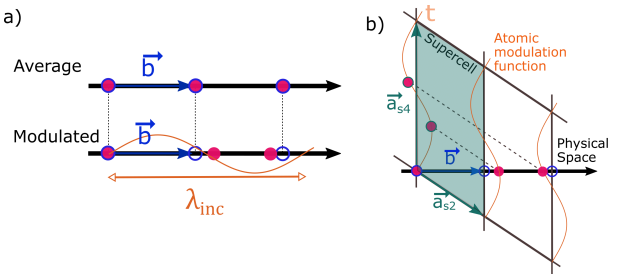

FIG. 4. (a) Schematic representation of an incommensurate phase in the physical space of dimension 3. The orange curve corresponds to the amplitude of the longitudinal incommensurate displacement along the axis, and blue and pink circles are respectively the mean and the incommensurate positions. (b) Superspace representation of dimension 3+1. The supercell in green is periodic and the orange curve represents the atomic modulation function along the internal dimension t of the superspace. The actual positions in the physical space of the atoms in pink circles are given by a horizontal cut.

this study at 80 K. For a sake of simplicity, we consider a chain of atoms of period b, modulated in position by a sinusoidal function $A\ \sin(q\ y)$ where $q = \frac{2\pi}{\lambda}$, λ/b is irrational number and A is the amplitude of the modulation. By introducing a perpendicular direction to the physical space, the incommensurate modulation function can be represented along the internal direction of the crystallographic superspace. The wavelength λ of the incommensurate modulation along $\boldsymbol{b}$ verifies $\lambda = \frac{b}{\beta}$. This defines a superspace cell characterized by the $\boldsymbol{a_{s2}}$, $\boldsymbol{a_{s4}}$ basic vectors. In this description, atomic position is no more coordinates but is defined by its atomic modulation function. The real position of the atoms represented by pink circles in the physical space is obtained by a one-dimensional cut of the periodic superspace [Fig. 4(b)] [29–31]. Solving the structure means determining the atomic modulation function of all the atoms of the mean three-dimensional unit cell as function of the period along the fourth dimension, which is called conventionally the variable t as defined in Fig. 4(b).

The reflection intensities including satellites were integrated using the program CrysAlis [18]. The structure model was constructed and refined using the program Jana2006 [28]. Only peaks with $I/\sigma > 6$ were used for this refinement (4296 main reflections and 8495 first order satellites). A two-step procedure was carried out. First, the average structure was refined against main reflection only and with isotropic atomic displacement parameters. Then the parameters of the average structure were fixed, and only the modulation parameters of all atoms were refined against both the main and satellite reflections. As only satellites of order 1 were observed, only one harmonic modulation wave per atom was necessary. The structure could be refined to a weighted R value of 0.061, 0.046, and 0.135 for all, main, and satellites reflections, respectively. CCDC-2269861 contains the supplementary crystallographic data for phase II at 80 K [21]. One way to analyze the structure in the superspace is to look at t-plots. A t-plot is constructed by looking at structural parameters like distances between two atoms as a function of t. The different relevant parameters d_{Pd-Pd}, α, Ψ, and ΔSb are defined in Fig. 5: d_{Pd-Pd} is the distance between the two palladium atoms within a dimer, α is an intramolecular angle of the molecule $Pd(dmit)_2$, Ψ is the intramolecular torsion angle between the two ethyl groups in the Et_2Me_2Sb cation and ΔSb is the displacement of the Sb atom along the $\boldsymbol{c}$ direction. In phase III, the two different values correspond to the values measured in two non-crystallographic equivalent dimers or cations. Table I summarizes the structural parameters in the three phases. The parameters in the high symmetry phase I (at 250 K) and in the low symmetry one III (at 25 K), are in agreement with the results reported previously in the literature by Nakao and Kato [2].

As shown in Fig. 6, strong modulation of the structure of the dimer as well as the cation can be observed. The position of the Sb atom exhibits a strong modulation in phase II with a displacement (ΔSb) from one-unit cell to another that can reach up to 0.35 Å. The torsion angle (Ψ) between the two ethyl groups in the Et_2Me_2Sb cation also shows a wide range of modulation.

It is noteworthy from Fig. 6 and Table I that the amplitude of the incommensurate modulations varies around the observed values in phase I and nearly reaches the ordered values of the periodic low symmetry phase III. This consistency arise from the fact that the locked low symmetry phase essentially involves to a jump of the modulation wave vector $\boldsymbol{q_s} = \beta\ \boldsymbol{b^*}$ to the commensurate one while retaining most of the structural features of the incommensurate modulation. However, this behavior is surprisingly not observed for the intermolecular Pd-Pd distance (d_{Pd-Pd}) between the two $Pd(dmit)_2$ units within the dimer [Fig. 6(d)]. According to [16, 17, 32, 33], the instability toward the charge

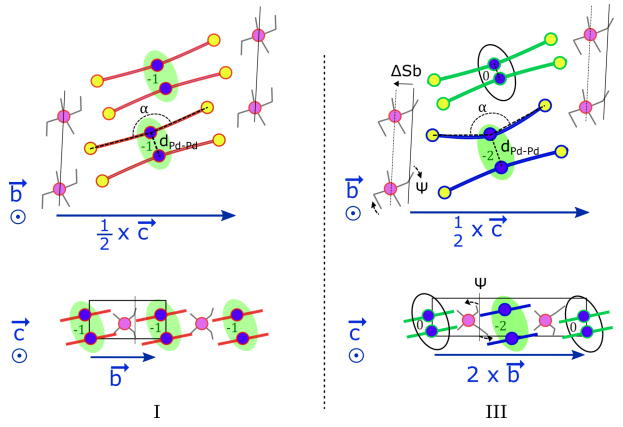

FIG. 5. Schematic representation of the structural ordering in the high symmetry phase C2/c and in the low symmetry phase $P2_1/c$. The symbols α, Ψ, d_{Pd-Pd}, and ΔSb correspond to molecular and dimer structural parameters which are significantly different in the high and in the low temperature phases.

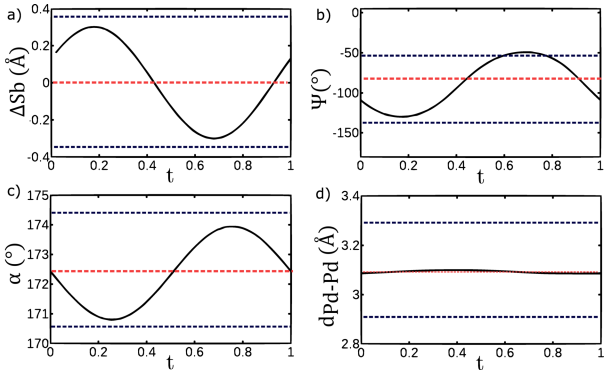

FIG. 6. t-plot of different structural parameters obtained at 80 K in phase II. (a) Positional modulated displacement ΔSb along the c direction of antinomy atom Sb in the Et_2Me_2Sb cation; (b) Modulation of the intramolecular torsion angle Ψ between the two ethyl groups in the Et_2Me_2Sb cation; (c) Rotational modulation of the internal angle in the molecule $Pd(dmit)_2$; (d) Distance d_{Pd-Pd} between the two $Pd(dmit)_2$ molecules in the dimer. The dotted lines in red and blue indicate the corresponding values in the high and low symmetric periodic phases, respectively.

separation (CS) state stems from a unique mechanism involving inversion of the HOMO-LUMO energy levels of the $Pd(dmit)_2$ molecule within the dimer. The charge transfer between the dimers is accompanied by a lattice distortion resulting in two types of dimer couples: a tight neutral dimer with four electrons occupying the two lower bonding levels and a loose divalent dimer with six electrons occupying the two lower bonding levels and one higher anti-bonding level. Both dimers exhibit spin singlet pairs which explain the diamagnetic nature of the CS phase. Consequently, a strong significant structural signature of the CS state is the Pd-Pd distance (d_{Pd-Pd}). Based on this structural analysis, it emerges that the amplitude of the Pd-Pd distance modulation in the incommensurate phase is negligible compared to the effective jump during the lock-in transition and the Pd-Pd distance is almost not changed compared to the high symmetry phase. Therefore, we can conclude that no CS is observed in the incommensurate phase and the average charge of the dimer is -1, similar to phase I.

TABLE I. Different characteristic structural parameters in phase I (250 K), phase III (25 K), and phase II (80 K) : the symbols d_{Pd-Pd}, α, Ψ, and ΔSb correspond to intramolecular and dimer structural parameters defined in Fig. 5. In phase III, the two different values correspond to the values measured in two non-crystallographic equivalent dimers or cations.

	Phase I (250 K)	Phase III (25 K)	Phase II (80 K)
d_{Pd-Pd}	3.13 Å	2.92 Å 3.32 Å	min 3.14 Å max 3.15 Å
α	172.5°	170.6° 174.4°	min 170.8° max 174.0°
Ψ	-88.2°	-142° -52°	min -130° max -50°
ΔSb	0	-0.37 Å +0.37 Å	min -0.30 Å max +0.30 Å

The modulation functions extracted from the structural analysis provide an explicit representation of the overall atomic modulation. However, given this findings, it is more informative to visualize the impact of the modulation on the structure in real space. Figure 7 shows the results of the incommensurate modulation over an extended distance corresponding to eight average unit cells along the $\boldsymbol{b}$ direction. The cation geometry undergoes a drastic modification with a significant modulation of the torsion angle Ψ. Additionally, the cation moves inside or outside the dimer, causing a bending of the $Pd(dmit)_2$ molecules, while the distance between the two molecules around the Pd atoms remains almost constant in phase II. We can therefore conclude that the frustration leading to incommensurate modulation arises from a very strong steric effect between the alkyl groups of the Et_2Me_2Sb cation and the terminal S atoms of the $Pd(dmit)_2$ molecule competing with the CS state of the low temperature phase. As temperature decreases, the amplitude of these modulations increases as illustrated by the increase of the intensity of the satellites shown in that temperature range in the figure 3. At $Tc = 66.5$ K, the system undergoes a lock-in phase transition. This phase transition is associated with the CS mechanism accompanied by a large structural change of the dimers.

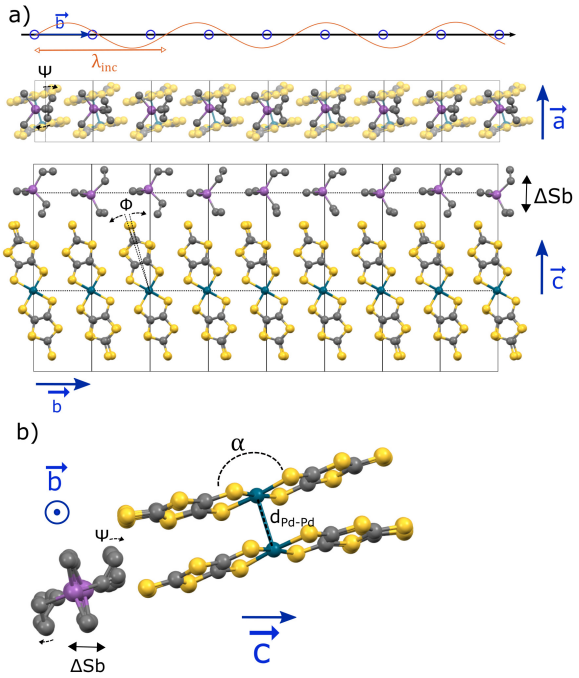

FIG. 7. (a) View of 8 adjacent unit cells of the incommensurate phase of $Et_2Me_2Sb[Pd(dmit)_2]_2$ shown in the real space. Effective atomic modulations with a period λ = b/β with β = 0.45 (represented by the orange sinusoidal curve) show the spatial variation of the intramolecular and intermolecular parameters, d_{Pd-Pd}, α, Ψ, Φ and ΔSb. (b) Side view along the incommensurate direction b showing the superposition of these same 8 adjacent unit cells.

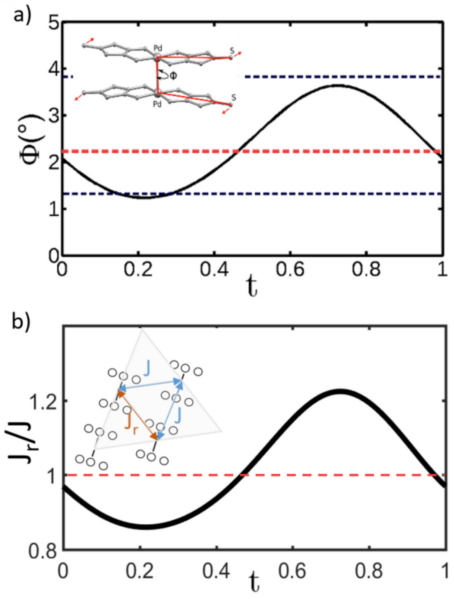

FIG. 8. (a) Modulation in phase II of the torsion angle. Red dotted lines and blue dotted line are respectively the torsion angles in phase I and phase III. Inset shows the definition of the torsion angle S-Pd-Pd-S characterizing the mismatch of overlap between the two molecules inside the dimer. (b) Estimated anisotropy parameter J_r/J of triangular lattice in phase II for different value of t. Inset shows the definition of the interdimer transfer integrals J_r and J.

V. INCOMMENSURATE DEGREE OF SPIN FRUSTRATION AND ITS MAGNETIC PROPERTIES

The dimer units within the anion layer are networked to form a quasi-triangular lattice [Fig. 1(c)]. The triangular lattice, resulting from the interdimer interactions, is approximately isosceles, allowing us to estimate the anisotropy of the triangular using the J_r/J ratio where J_r and J are the interdimer transfer integrals as defined in Fig. 1(c). In this system, these interdimer interactions are related to the degree of the arch-shaped molecular distortion that is reflected in the overlap of the two $Pd(dmit)_2$ molecules within the dimer [15]. The deviation from perfect overlap can be estimated by the change in the S-Pd-Pd-S torsion angle (Φ) [inset of Fig. 8(a)]. Figure 8(a) represents the t-plot of the torsion angle (Φ) and Fig. 7(a) illustrates its modulation in real space. The average value in phase I and the two distinct values in phase III are similar to those reported in reference [15] and its variation follows the variation of the intramolecular angle (α) since the modulation of the torsion also originates from the strong steric effect between the cation and the terminal S atoms. It has been demonstrated that the interdimer transfer integrals J_r and J are linearly correlated with Φ [15]. In the high symmetry phase I, Φ = 2.2 ° and $J_r = J$ = 25 meV, describing an equilateral triangular lattice with an anisotropy parameter J_r/J = 1. Based on the work presented in [15], we can estimate J_r and J for different values of Φ observed in the incommensurate phase II. At the minimum Φ = 1.2 °, the estimated values are J_r = 24.1 meV and J = 28.2 meV and at the maximum Φ = 3.8 °, J_r = 27.6 meV and J = 22.0 meV. In the incommensurate phase II, the anisotropy parameter J_r/J modulates from approximately 0.86 to 1.25, as illustrated by the t-plot of J/J in Fig. 8(b).

Spin frustration occurs in systems where the interactions between the spins on a lattice cannot be simultaneously satisfied. In an equilateral triangular lattice, it is impossible to arrange the spins in a way that every pair of neighboring spins aligns anti-parallel, as would be the case in an anti-ferromagnetic system. Because the degree of anisotropy of triangular lattice is modulated in phase II, we can conclude that the incommensurate phase is characterized by an incommensurate modulation of the degree of spin frustration. This finding is consistent with the susceptibility curve observed in phase II, as shown in Fig. 1(d). The degree of anisotropy on the triangular lattice has been established as the most important parameter for explaining the magnetic properties. In phase I, the temperature dependence of the magnetic susceptibility can be described by a model of a spin-1/2 Heisenberg antiferromagnet on a triangular lattice with the exchange

coupling $J_{exch}/k_B = 240$ K. The exchange coupling J_{exch} appears to slightly increase with temperature above 100 K [7]. However, neither a spin-1/2 Heisenberg model nor an exponential drop due to non-magnetism can be applied to χ(T) in phase II. The observed incommensurate degree of spin frustration observed in phase II is most likely the origin of this weak anomalous variation of the magnetic susceptibility.

VI. INFRARED VIBRATIONAL SPECTROSCOPY IN THE INCOMMENSURATE PHASE

The charge and the structure information can be captured via vibrational spectroscopy [34]. Temperature dependence of the reflectivity spectra with the polarization parallel to the $\boldsymbol{a}$ axis has been measured in the infrared (IR) region to study the charge and the local structure of the Pd(dmit)$_2$ dimer. Figure 9(a) shows the temperature dependence of the reflectivity spectra in the C=C stretching mode's energy range. When Pd(dmit)$_2$ molecules form a dimer, four vibrational modes emerge as a result of an in-phase and an out-of-phase combination of IR- and Raman-active C=C stretching modes of the Pd(dmit)$_2$ molecules. The so-called B and C modes are IR-active [34] and observed as double peak structures in the spectra at 120 K (phase I) in Fig. 9(a). With lowering the temperature, there is little change of the spectral shape at *Ti*, while a large change has been observed at *Tc*, which is consistent with the reported work [34]. Little change of the spectral shape at *Ti* indicates that the charge of the monomer and dimer remains -0.5 and -1, respectively, and the Pd–Pd distance in the dimer is unchanged at the phase transition between phases I and II. The structure and charge of the dimer in phase II are very similar to phase I in agreement with the structural and magnetic studies presented above. However, small signs of incommensurate modulation have been indeed observed in an other energy range. In phase I, single peak structure is located around 920 cm^{-1} as shown in Fig. 9(b). This mode can be assigned as the C-S stretching mode as schematically shown in the inset of Fig. 9(b), based on the quantum chemical calculation by Gaussian 16 [35]. This structure shows almost no change in phase II, but it splits into several peaks in phase III. The splitting of the peak is expected because there are at least two kinds of dimers in phase III. It should be noted that the intensity of a weak IR-active mode at around 932 cm^{-1} increases with lowering temperature in the phase II and disappeared below *Tc*. The crystal structure of phase II shows that the intramolecular structural parameters such as the bending angle (α) are strongly modulated leading to a positional modulation of the terminal S atom [Fig. 7(b)] that could affect the IR spectrum. The appearance of this small peak around 932 cm^{-1} only in phase II is a sign of such modulation. Two possible assignments of this mode can be proposed. The

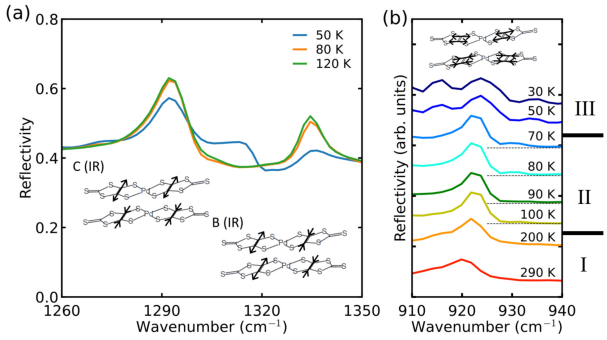

FIG. 9. Temperature dependence of reflectivity spectra with the polarization parallel to the $\boldsymbol{a}$ axis. (a) Spectra in the C=C stretching mode at 120 K (phase I), 80 K (phase II), and 50 K (phase III). The B and C bands are centered around 1332 and 1292 cm^{-1} at 120 K, respectively. Insets show schematic atomic motions of the B and C modes of the dimer. (b) Temperature dependence in the energy range of the C-S stretching mode. A small peak structure appears around 932 cm^{-1} in phase II. The horizontal dashed lines are guide to the eyes. Inset shows schematic atomic motions of the IR-active C–S stretching mode of the dimer.

first is the disappearance of the inversion center from the Pd(dmit)$_2$ dimer, causing the Raman mode to become IR active. The second one is the change of the spectral weight of the Et$_2$Me$_2$Sb mode due to the steric interaction between Et$_2$Me$_2$Sb and Pd(dmit)$_2$. Judging from the weak intensity of the Et$_2$Me$_2$Sb mode from the calculation, the first one is a more plausible mechanism. In addition, it should be noted that Ref. [32] has reported a Et$_2$Me$_2$Sb mode around 1405 cm^{-1} which is observed only below *Ti*, suggesting the close relation between the structure of Et$_2$Me$_2$Sb and Pd(dmit)$_2$ in phases II and III.

VII. DISCUSSIONS

The Cs[Pd(dmit)$_2$] salt presents a phase transition from a metallic phase to the CS phase [2], without any intermediate incommensurate phase. This directs our attention to the origin of the different sequences of phases in these two salts. The Cs cation is spherical and the steric effect is either absent or very small compared to the Et$_2$Me$_2$Sb salt where the hook shape of the cation induces a strong steric effect. The high temperature phase in Cs and Et$_2$Me$_2$Sb salts are quite different. In the high temperature metallic phase in the Cs salt, the spin fluctuation is suppressed due to itinerant electrons and as a consequence, the Cs salt does not show any spin frustration which is a characteristic of the phase I of Et$_2$Me$_2$Sb salt. Based on these observations and our structural analysis of the incommensurate phase II, we can conclude that the origin of the incommensurate phase in Et$_2$Me$_2$Sb salt is therefore the result of the competition between the steric effect, the magnetic frustration and the CS state.

A photoinduced phase transition (PIPT) has been studied using the time-resolved IR spectroscopy in this crystal [36–38]. After the photoexcitation in phase III, it is found that a high-temperature phase emerges with a two-step sequences. However it is not clear whether it is phase I or II. The slow emergence of the photoinduced state is considered to originate from the lattice distortion induced by the cation. The lattice distortion plays a key role in the mechanism stabilizing the photoinduced phase as already reported in the photoinduced metallic phase in (BEDT-TTF)$_3$X$_2$, (X = ReO_4 and ClO_4) or in (EDOTTF)$_2$X, (X = PF_6 and SbF_6) [39–41]. The lattice distortion is controlled by the shape of the cation in [Pd(dmit)$_2$] salts. In the case of the Cs[Pd(dmit)$_2$] salt [38] where the cation Cs is spherical without a hook, the emergence of the photoinduced high temperature state is very fast and occurs in a single step. On the other hand, the two-step photoinduced processes observed in the Et_2Me_2Sb salt is due to the steric effect between the hook shape Et_2Me_2Sb cations and Pd(dmit)$_2$ anions. To interpret the PIPT, two highly symmetric phases should be taken into account: the incommensurate C2/c(0β0)s0 phase II and the periodic C2/c phase I. There is a possibility that the short time process corresponds to the formation of the intermediate incommensurate phase, the longtime process to the erasing of the incommensurate modulation. Such a suppression of the incommensurate modulation by light was reported previously by Collet et al. [42] in a spin cross-over system.

VIII. CONCLUSION

In a general way, an incommensurate phase arises from a frustration between competitive forces. The case of the two-dimensional triangular lattice of $Et_2Me_2Sb[Pd(dmit)_2]_2$, charges and spins interact with one another in a manner that leads to frustration. The high temperature phase I is characterized by a geometric frustration due to its 2D equilateral triangular lattice. On the other hand, the low temperature phase III presents two different dimers with two distinct charges in the CS state. High resolution x-ray measurements performed on single crystal revealed the presence of an intermediate incommensurate phase II. The temperature dependent phase diagram was determined and we characterized the superspace group of the new phase. The structure was solved and refined using the superspace formalism and the main features of this phase was confirmed by the measurement of the IR vibrational spectrum. In this study, we have identified an intermediate phase, that does not undergo the CS transition, between previously characterized phases, phase I and phase III. Within this phase II, the strong steric interaction as well as the degree of spin frustration are incommensurately modulated. The competition between the steric effect, the magnetic frustration and the CS state leads to the emergence of the incommensurate modulation in phase II. As a consequence, a highly distinctive order appears, where the degree of spin frustration must be aperiodically modulated. Further investigation should be carried out to reveal the spin structure in phase II of $Et_2Me_2Sb[Pd(dmit)_2]_2$.

ACKNOWLEDGMENTS

We thank Hervé Cailleau for initiating this project, Loic Toupet for the experimental support, and Oliver Perez, Philippe Rabiller and Seiko Ohira-Kawamura for fruitful discussions. This work was partly supported by JSPS KAKENHI Grant Number JP19K05405.

[1] R. Kato, Chemical Reviews **104**, 5319 (2004).
[2] A. Nakao and R. Kato, Journal of the Physical Society of Japan **74**, 2754 (2005).
[3] R. Kato, Bulletin of the Chemical Society of Japan **87**, 355 (2014).
[4] M. F. Collins and O. A. Petrenko, Canadian Journal of Physics **75**, 605 (1997).
[5] L. Balents, Nature **464**, 199 (2010).
[6] K. Kanoda and R. Kato, Annual Review of Condensed Matter Physics **2**, 167 (2011).
[7] M. Tamura and R. Kato, Journal of Physics: Condensed Matter **14**, L729 (2002).
[8] M. Tamura, A. Nakao, and R. Kato, Journal of the Physical Society of Japan **75**, 093701 (2006).
[9] T. Itou, A. Oyamada, S. Maegawa, and R. Kato, Nature Physics **6**, 673 (2010).
[10] R. Coldea, D. A. Tennant, and Z. Tylczynski, Physical Review B **68**, 134424 (2003).
[11] K. Nawa, D. Hirai, M. Kofu, K. Nakajima, R. Murasaki, S. Kogane, M. Kimata, H. Nojiri, Z. Hiroi, and T. J. Sato, Physical Review Research **2**, 043121 (2020).
[12] T. Itou, A. Oyamada, S. Maegawa, M. Tamura, and R. Kato, Physical Review B **77**, 104413 (2008).
[13] S. Yamashita, T. Yamamoto, Y. Nakazawa, M. Tamura, and R. Kato, Nature Communications **2**, 275 (2011).
[14] S. Fujiyama and R. Kato, Physical Review Letters **122**, 147204 (2019).
[15] R. Kato and C. Hengbo, Crystals **2**, 861 (2012).
[16] M. Tamura and R. Kato, Chemical Physics Letters **387**, 448 (2004).
[17] M. Tamura, K. Takenaka, H. Takagi, S. Sugai, A. Tajima, and R. Kato, Chemical Physics Letters **411**, 133 (2005).
[18] Crysalis pro. agilent technologies uk ltd, yarnton, england, (2011).
[19] G. M. Sheldrick, Acta Crystallographica Section A Foundations and Advances **71**, 3 (2015).
[20] G. M. Sheldrick, Acta Crystallographica Section A Foundations of Crystallography **64**, 112 (2007).
[21] Cif files can be obtained free of charge via www.ccdc.cam.ac.uk/conts/retrieving.html (or from

the Cambridge Crystallographic Data Centre, 12 Union Road, Cambridge CB2 1EZ, UK; fax: (+44) 1223-336-033; or deposit@ccdc.ca.ac.uk).

[22] T. Janssen, A. Janner, A. Looijenga-Vos, and P. M. de Wolff, in International Tables for Crystallography , 907 (2006).

[23] H. T. Stokes, B. J. Campbell, and S. van Smaalen, Acta Crystallographica Section A Foundations of Crystallography **67**, 45 (2010).

[24] S. van Smaalen, B. J. Campbell, and H. T. Stokes, Acta Crystallographica Section A Foundations of Crystallography **69**, 75 (2012).

[25] H. T. Stokes, D. M. Hatch, and B. J. Campbell, Iso(3+d)d, isotropy software suite, iso.byu.edu., (2022).

[26] R. A. Cowley and A. D. Bruce, Journal of Physics C: Solid State Physics **11**, 3577 (1978).

[27] R. Blinc and A. P. Levanyuk, *Incommensurate Phases in Dielectrics, Vols. 1 and 2* (R. Blinc,A. P. Levanyuk, Amsterdam, 1986).

[28] V. Petříček, M. Dušek, and L. Palatinus, Zeitschrift für Kristallographie - Crystalline Materials **229**, 345 (2014).

[29] T. Janssen and A. Janner, Acta Crystallographica Section B Structural Science, Crystal Engineering and Materials **70**, 617 (2014).

[30] T. Janssen, G. Chapuis, and M. de Boissieu, *Aperiodic Crystals: From Modulated Phases to Quasicrystals* (Oxford University Press, Oxford, 2007).

[31] S. V. Smaalen, *Incommensurate Crystallography* (Oxford University Press, Oxford, 2007).

[32] H. Seo, T. Tsumuraya, M. Tsuchiizu, T. Miyazaki, and R. Kato, Journal of the Physical Society of Japan **84**, 044716 (2015).

[33] T. Yamamoto, M. Tamura, K. Yakushi, and R. Kato, Journal of the Physical Society of Japan **85**, 104711 (2016).

[34] T. Yamamoto, Y. Nakazawa, M. Tamura, T. Fukunaga, R. Kato, and K. Yakushi, Journal of the Physical Society of Japan **80**, 074717 (2011).

[35] M. J. Frisch, G. W. Trucks, H. B. Schlegel, G. E. Scuseria, M. A. Robb, J. R. Cheeseman, G. Scalmani, V. Barone, G. A. Petersson, H. Nakatsuji, X. Li, M. Caricato, A. V. Marenich, J. Bloino, B. G. Janesko, R. Gomperts, B. Mennucci, H. P. Hratchian, J. V. Ortiz, A. F. Izmaylov, J. L. Sonnenberg, D. Williams-Young, F. Ding, F. Lipparini, F. Egidi, J. Goings, B. Peng, A. Petrone, T. Henderson, D. Ranasinghe, V. G. Zakrzewski, J. Gao, N. Rega, G. Zheng, W. Liang, M. Hada, M. Ehara, K. Toyota, R. Fukuda, J. Hasegawa, M. Ishida, T. Nakajima, Y. Honda, O. Kitao, H. Nakai, T. Vreven, K. Throssell, J. A. Montgomery, Jr., J. E. Peralta, F. Ogliaro, M. J. Bearpark, J. J. Heyd, E. N. Brothers, K. N. Kudin, V. N. Staroverov, T. A. Keith, R. Kobayashi, J. Normand, K. Raghavachari, A. P. Rendell, J. C. Burant, S. S. Iyengar, J. Tomasi, M. Cossi, J. M. Millam, M. Klene, C. Adamo, R. Cammi, J. W. Ochterski, R. L. Martin, K. Morokuma, O. Farkas, J. B. Foresman, and D. J. Fox, Gaussian16 (2016), gaussian Inc. Wallingford CT.

[36] T. Ishikawa, N. Fukazawa, Y. Matsubara, R. Nakajima, K. Onda, Y. Okimoto, S. Koshihara, M. Tamura, R. Kato, M. Lorenc, and E. Collet, physica status solidi c **6**, 112 (2008).

[37] T. Ishikawa, N. Fukazawa, Y. Matsubara, R. Nakajima, K. Onda, Y. Okimoto, S. Koshihara, M. Lorenc, E. Collet, M. Tamura, and R. Kato, Physical Review B **80**, 115108 (2009).

[38] N. Fukazawa, T. Tanaka, T. Ishikawa, Y. Okimoto, S. Koshihara, T. Yamamoto, M. Tamura, R. Kato, and K. Onda, The Journal of Physical Chemistry C **117**, 13187 (2013).

[39] N. Takubo, N. Tajima, H. M. Yamamoto, H. Cui, and R. Kato, Physical Review Letters **110**, 227401 (2013).

[40] N. Fukazawa, M. Shimizu, T. Ishikawa, Y. Okimoto, S. Koshihara, T. Hiramatsu, Y. Nakano, H. Yamochi, G. Saito, and K. Onda, The Journal of Physical Chemistry C **116**, 5892 (2012).

[41] M. Servol, N. Moisan, E. Collet, H. Cailleau, W. Kaszub, L. Toupet, D. Boschetto, T. Ishikawa, A. Moréac, S. Koshihara, M. Maesato, M. Uruichi, X. Shao, Y. Nakano, H. Yamochi, G. Saito, and M. Lorenc, Physical Review B **92**, 024304 (2015).

[42] E. Collet, H. Watanabe, N. Bréfuel, L. Palatinus, L. Roudaut, L. Toupet, K. Tanaka, J.-P. Tuchagues, P. Fertey, S. Ravy, B. Toudic, and H. Cailleau, Physical Review Letters **109**, 257206 (2012).